

# Structure Functions, the Gluon Density, and PQCD Tests

Richard Cross  
*University of Wisconsin-Madison*  
*For the ZEUS collaboration*

Measurements of the proton structure function  $F_2$  for  $0.11 < Q^2 < 20000 \text{ GeV}^2$  and  $1.2 \times 10^{-5} < x < 0.65$  from ZEUS 1994-1997 measurements are presented. From ZEUS 1994 and 1995  $F_2$  data the slopes  $dF_2/d \ln Q^2$  at fixed  $x$  and  $d \ln F_2/d \ln(1/x)$  for  $x < 0.01$  at fixed  $Q^2$  are derived. For the latter E665 data are also used. The transition region in  $Q^2$  is explored using the simplest non-perturbative models and NLO QCD. The data at very low  $Q^2 \leq 0.65 \text{ GeV}^2$  are described successfully by Regge theory. From a NLO QCD fit to ZEUS data the gluon density in the proton is extracted in the range  $3 \times 10^{-5} < x < 0.7$ . Data from NMC and BCDMS constrain the fit at large  $x$ . Assuming the NLO QCD description to be valid down to  $Q^2 \sim 1 \text{ GeV}^2$ , it is found that the  $q\bar{q}$  sea distribution is still rising at small  $x$  and the lowest  $Q^2$  values whereas the gluon distribution is strongly suppressed. Preliminary ZEUS 1996-1997  $F_2$  measurements are also presented.

## I. INTRODUCTION

The deep inelastic scattering process is used to probe the structure of nucleons. Ultra-high energy transfers are achieved at the DESY laboratory, in Hamburg, Germany, where 820 GeV protons are collided with 27.5 GeV positrons for a center-of-mass energy  $\sqrt{s}=300 \text{ GeV}$ . The deep inelastic scattering (DIS) process at HERA is illustrated in Fig. 1. The variables are related by  $Q^2 = sxy$ .

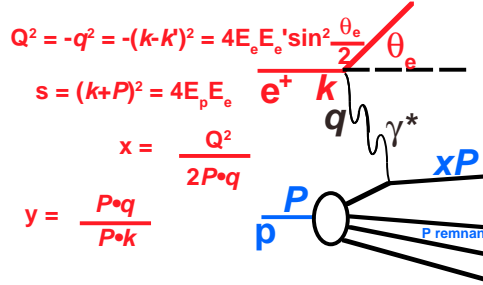


FIG. 1.

In the  $Q^2$  range examined here the double differential cross-section for single virtual-photon exchange in DIS is given by

$$\frac{d^2\sigma}{dx dQ^2} = \frac{2\pi\alpha^2}{xQ^4} \left[ 2(1-y) + \frac{y^2}{1+R} \right] F_2(x, Q^2) [1 + \delta_r(x, Q^2)], \quad (1)$$

where  $R$  is related to the longitudinal structure function  $F_L$  by  $R = F_L/(F_2 - F_L)$  and  $\delta_r$  gives the radiative corrections to the Born cross-section, which in this kinematic range are at most 10%. For  $R$  we take values given by the BKS model [2].

Measurements of  $F_2$  for  $0.11 < Q^2 < 20000 \text{ GeV}^2$  are presented. The rapid rise of  $F_2$  at low  $x$  can be seen. The  $F_2$  measurements are fit to pQCD and Regge motivated functions. These measurements illuminate the region where QCD breaks down because  $Q^2 \rightarrow 0$ .

The ZEUS 1995  $F_2$  measurement increased the kinematic coverage in the low  $x$  and  $Q^2$  region. The coverage for  $Q^2$  between 0.11 and 0.65  $\text{GeV}^2$  was made possible by the installation of a small electromagnetic sampling calorimeter, the Beam Pipe Calorimeter (BPC), at small positron scattering angles. The proton structure function  $F_2$  and the total  $\gamma^*p$  cross-section have been published [1]. Results for  $Q^2$  between 0.6 and 17  $\text{GeV}^2$  were made possible by a set of runs in 1995 with a mean interaction vertex shifted 70 cm in the direction of the incoming electron. The QCD fits presented also used data from the 1994 ZEUS  $F_2$  measurement and from E665.

These data sets are fit using QCD and Regge functional forms. The slopes are extracted. The combined sample is fit using DGLAP. The results of the DGLAP fit are used to extract the gluon density.

Also shown are preliminary results the 1996-97 ZEUS  $F_2$  measurements. There is reasonable agreement with the 1994 ZEUS results. The 1996-97 measurement fills in the region between the 1994 ZEUS results and results from fixed target experiments. The 1996-97 results also have data at higher  $Q^2$ .

## II. THE ZEUS DETECTOR.

ZEUS [3] is a multi-purpose magnetic detector. The primary components used in these analyses are the uranium calorimeter, the beam pipe calorimeter, tracking detectors, and luminosity monitors. The coordinate system is defined such that the  $z$ -axis follows the proton direction, and the origin is the nominal  $ep$  interaction point.

The ZEUS compensating uranium-scintillator calorimeter covers the polar angle region  $2.6^\circ < \theta < 176.1^\circ$  with full azimuthal coverage over this region. Its energy resolution for electromagnetic showers is  $\sigma_E/E \simeq 18\%/\sqrt{E(\text{GeV})}$ , and for hadronic showers is  $\sigma_E/E \simeq 35\%/\sqrt{E(\text{GeV})}$ . The Beam Pipe Calorimeter is placed outside the main Uranium calorimeter and at an angle of almost  $180^\circ$  so that it can measure outgoing electrons at  $Q^2$  down to  $0.1 \text{ GeV}^2$ . The ZEUS tracking detectors primarily provide vertex reconstruction. ZEUS has cylindrical central tracking chambers and forward and rear tracking chambers, operating in a solenoidal 1.43 T magnetic field.

The luminosity is determined from the rate of Bethe-Heitler bremsstrahlung ( $ep \rightarrow ep\gamma$ ) events in detectors near the beamline.

## III. $F_2$ FITS AND THE TRANSITION REGION.

Three ZEUS  $F_2$  data samples are used to examine the transition region. The ZEUS 1994 DIS ZEUS sample required an electron of 10 GeV in the uranium calorimeter,  $35 \text{ GeV} < E - p_z < 65 \text{ GeV}$ , and an event vertex in the range  $40\text{cm} < Z_{\text{vertex}} < 160\text{cm}$ . The 1995 shifted vertex sample used a different nominal vertex, so the event vertex is required to lie in the range  $40\text{cm} < Z_{\text{vertex}} < 160\text{cm}$ . The 1995 Beam Pipe Calorimeter sample required that an electron be contained in the BPC rather than the uranium calorimeter. Because the BPC is at smaller  $\eta$  than the uranium calorimeter, the BPC sample can reach lower  $Q^2$ .

Low  $Q^2$  ( $Q^2 < 10\text{GeV}^2$ )  $F_2$  results at ZEUS show the transition region from pQCD to the Regge region. 1995 BPC data are binned in  $W^2$  and fit to a Donnachie-Landshoff [4] Regge parameterization of the form

$$\sigma_{\text{tot}}^{\gamma P}(W^2) = A_R(W^2)^{\alpha_R-1} + A_P(W^2)^{\alpha_P-1}$$

where  $P$  and  $R$  denote the Pomeron and Reggeon contributions. This is the ZEUSREGGE curve in figure 2.

Results from the 1994  $F_2$ , 1995 shifted vertex and E665 are also fit with the QCD based model. The kinematic range covered by this data is  $3 \times 10^{-5} < x < 0.7$  and  $0.9 < Q^2 < 5000 \text{ GeV}^2$ . This data is fit by solving the DGLAP evolution equations at NLO in the  $\overline{\text{MS}}$  scheme [5].

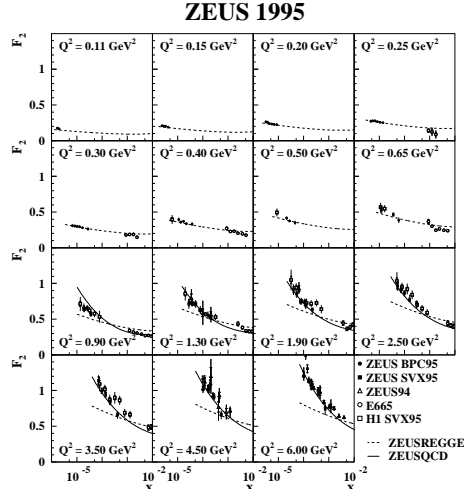


FIG. 2. Low  $Q^2$   $F_2$  data for different  $Q^2$  bins. A Regge inspired fit (dashed lines) to the BPC95 data is shown. At larger  $Q^2$  values a NLO QCD fit to the ZEUS data is also shown.

The 1994, 1995 and E665 samples are binned in  $Q^2$  and their slopes were extracted. These slopes are compared with QCD and Regge predictions. A GRV parameterization and the ZEUS QCD fit are shown for the higher  $Q^2$  data. For the low  $Q^2$  region the Regge fit to ZEUS data and a global Donnachie-Landshoff [4] fit are shown. Neither type of parameterization can describe the data in the transition region from high to low  $Q^2$ .

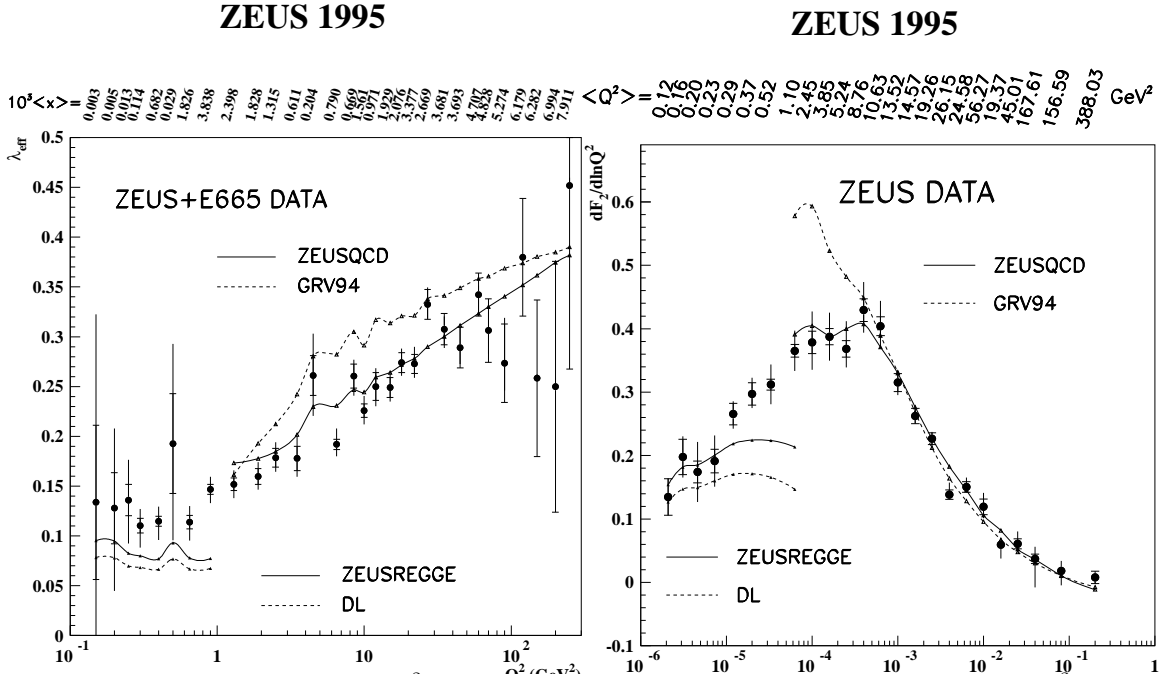


FIG. 3.  $d \ln F_2 / d \ln(1/x)$  as a function of  $Q^2$  calculated by fitting ZEUS and E665  $F_2$  data in bins of  $Q^2$  to the functional form  $Ax^{-\lambda_{eff}}$  (left).  $dF_2/d \ln Q^2$  as a function of  $x$  calculated by fitting ZEUS  $F_2$  data in bins of  $x$  to the functional form  $a + b \ln Q^2$  (right). The inner error bar shows the statistical error and the outer the total statistical and systematic error added in quadrature. In a  $Q^2$  bin  $\langle x \rangle$  is calculated from the weighted mean of  $\ln x$ . The linked points labelled DL and GRV94 are from the Donnachie-Landshoff Regge fit [4] and the GRV94 NLO QCD fit [7]. In both cases the points are obtained using the same weighted range of  $x$  as for the experimental data.

The ZEUS94 [6] and the 1995 shifted vertex data are fit in order to extract the gluon and quark densities at low  $x$ . They are fit by solving the DGLAP [8] evolution equations in NLO in the  $\overline{\text{MS}}$  scheme [5]. For this fit the starting scale is  $Q_0^2 = 7 \text{ GeV}^2$ . For data with  $Q^2 < 7 \text{ GeV}^2$ , backwards evolution in  $Q^2$  are performed. The gluon distribution ( $xg$ ),

the sea quark distribution ( $xS$ ) and the difference of up and down quarks in the proton ( $x\Delta_{ud}$ ) are parameterised as

$$\begin{aligned}
 xg(x, Q_0^2) &= A_g x^{\delta_g} (1-x)^{\eta_g} (1 + \gamma_g x) \\
 xS(x, Q_0^2) &\equiv 2x(\bar{u} + \bar{d} + \bar{s}) = A_s x^{\delta_s} (1-x)^{\eta_s} (1 + \varepsilon_s \sqrt{x} + \gamma_s x) \\
 x\Delta_{ud}(x, Q_0^2) &\equiv x(u + \bar{u}) - x(d + \bar{d}) = A_\Delta x^{\delta_\Delta} (1-x)^{\eta_\Delta}.
 \end{aligned}
 \tag{2}$$

The input valence distributions  $xu_v = x(u - \bar{u})$  and  $xd_v = x(d - \bar{d})$  at  $Q_0^2$  are taken from the parton distribution set MRS(R2) [9]. As for MRS(R2) we assume that the strange quark distribution is a given fraction  $K_s = 0.2$  of the sea at the scale  $Q^2 = 1\text{GeV}^2$ . The gluon normalization,  $A_g$ , is fixed by the momentum sum rule, that is, the total momentum fraction carried by quarks and gluons is required to add up to unity. There are 11 free parameters in the fit.

The fit yields a gluon distribution that rises dramatically as  $x$  decreases for  $Q^2$  of  $20\text{GeV}^2$ . The gluon distribution is consistent with 0 for  $Q^2$  of  $1\text{GeV}^2$ . It is not constrained to be greater than 0 in the fit. A negative gluon distribution is not in contradiction with NLO QCD as long as the cross sections calculated from the parton distributions are positive for all  $x$  and  $Q^2$  in the fitted kinematic region. This is the case for the fit values shown here. The sea quark distribution rises at low  $x$  even for  $Q^2$  of  $\text{GeV}^2$ . This can be interpreted as higher energy gluons generating  $q\bar{q}$  pairs.

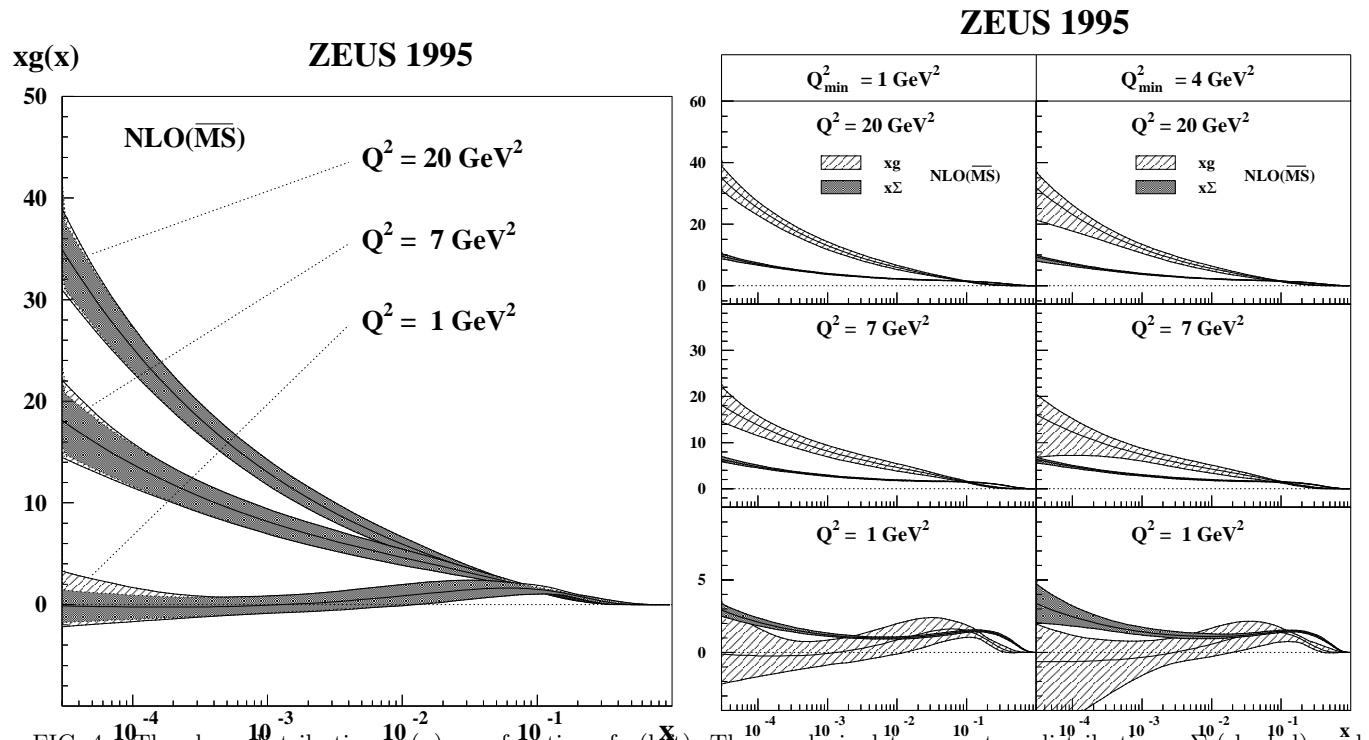


FIG. 4. The gluon distribution  $xg(x)$  as a function of  $x$  (left). The quark singlet momentum distribution,  $x\Sigma$  (shaded), and the gluon momentum distribution,  $xg(x)$  (hatched), as functions of  $x$  at fixed values of  $Q^2 = 1, 7$  and  $20 \text{ GeV}^2$  (right). The error bands correspond to the quadratic sum of all error sources considered for each parton density.

#### IV. 1996-97 $F_2$ .

The ZEUS 1996-1997  $F_2$  measurement is split into two samples. The high  $Q^2$  measurement uses the full  $27.4\text{pb}^{-1}$  of data taken in 1996-1997 run. The low  $Q^2$  measurement uses only  $6.8\text{pb}^{-1}$  of data. The combined measurements cover a  $Q^2$  range  $1.5 - 20000\text{GeV}^2$  and an  $x$  range of  $2.6 \times 10^{-5} < x < 0.65$ . Most bins have systematic errors of 3-4%. At high and low  $y$ , the error is as high as 10%. The high  $Q^2$  measurement has better statistics than the 1994 ZEUS  $F_2$  measurement.

The data was taken by requiring a positron with energy  $E_e > 10$  GeV. The accepted events were also required to have  $44 \text{ GeV} < E - p_z < 68 \text{ GeV}$ , and an event vertex in the range  $-50 \text{ cm} < z < 50 \text{ cm}$ .

The efficiency of the cuts is determined by comparing the data to a Monte Carlo that used the CTEQ4D parton densities. Figure 5 shows a comparison of several data and Monte Carlo quantities. The efficiency of the cuts as determined by Monte Carlo is 90%.

### ZEUS Preliminary 1996 - 1997

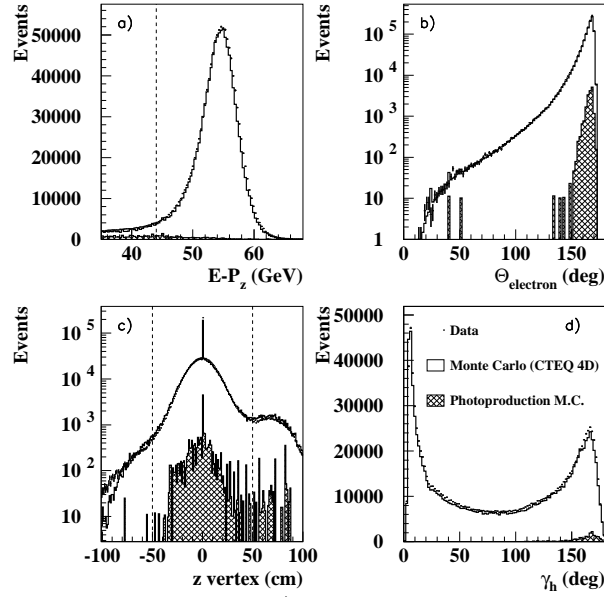


FIG. 5. a)  $E - P_z$ , b) angle of the measured electron, c) the  $z$  position of the event vertex, and d) the angle of the hadronic system. The Monte Carlo (histograms) are normalised to the luminosity of the data (dots). Data and MC show good agreement. The cuts requiring energy greater than 45 GeV (a) and an event vertex between + 50 cm in  $z$  and - 50 cm in  $z$  (c) are shown.

The ZEUS 1996-1997  $F_2$  data sample fills in many of the gaps between fixed target experiments and the 1994 ZEUS  $F_2$  sample. The errors are smaller than the 1994 sample. The 1996-1997 sample shows agreement with the 1994 sample and with previous fixed target experiments.

For a fixed  $Q^2$ , the ZEUS 1996-1997  $F_2$  rises dramatically as  $x$  decreases (see Figures 6 and 7). Also, for a fixed  $x$ ,  $F_2$  rises with  $Q^2$  (see Figure 8).

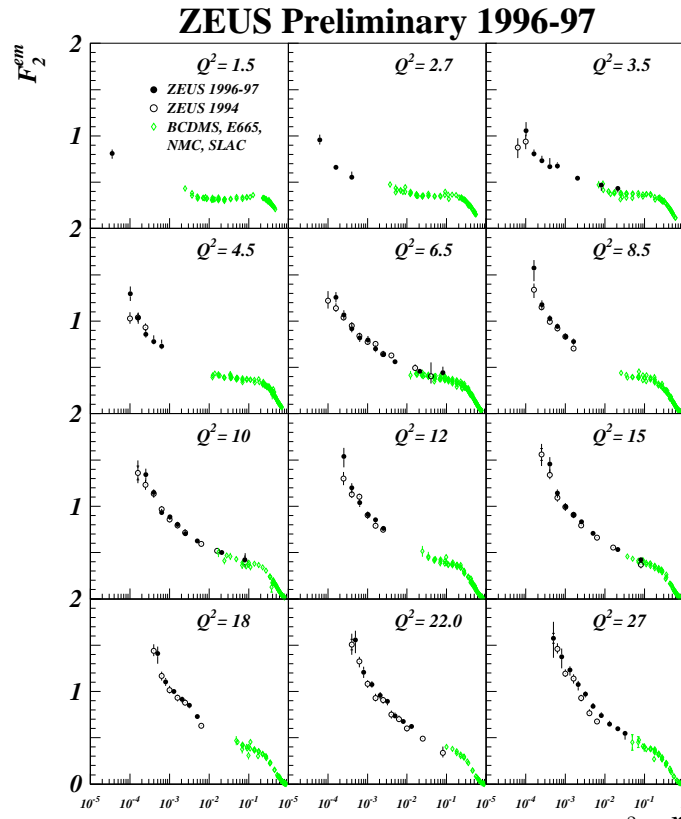


FIG. 6. ZEUS 1996 1997  $F_2$  measurement at low  $Q^2$ .  $x$

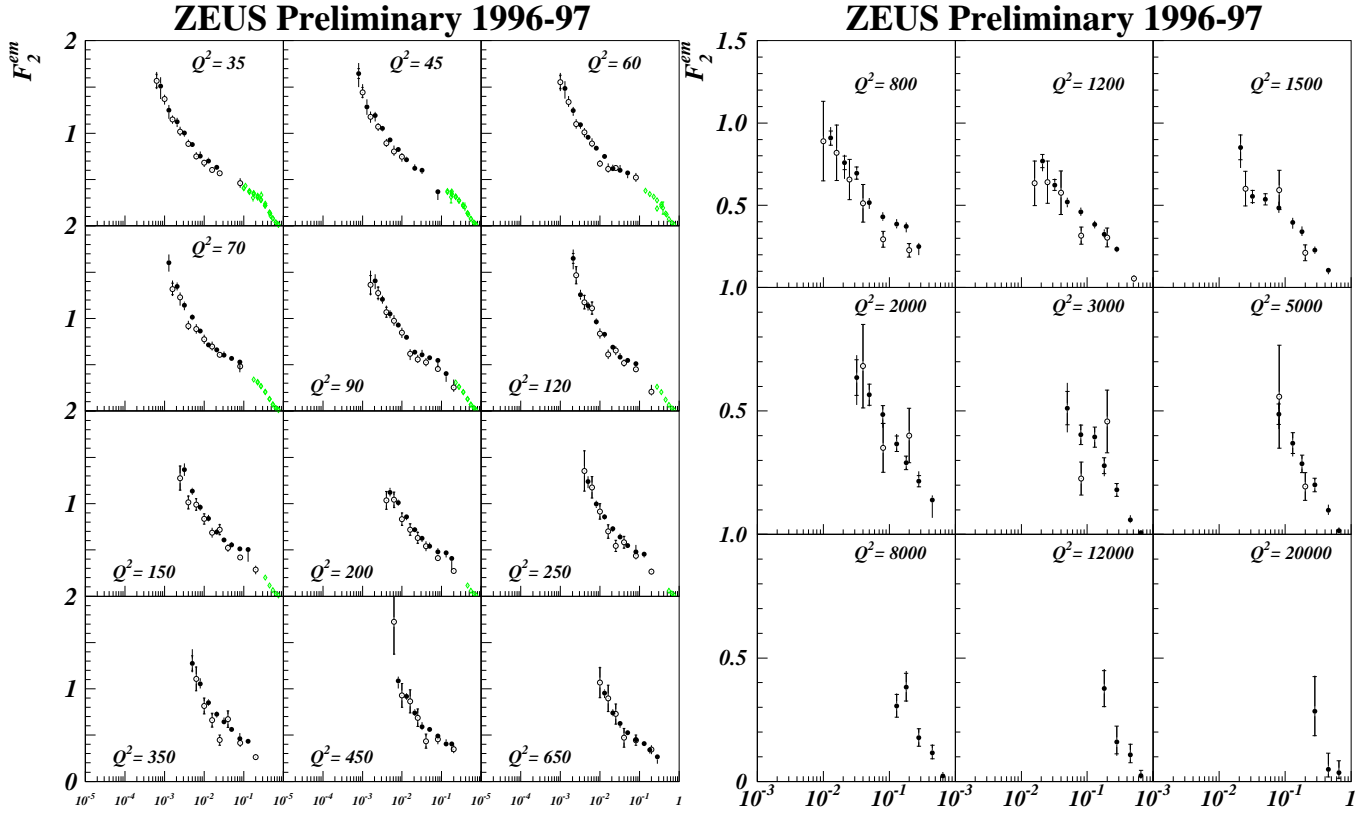


FIG. 7. ZEUS 1996 1997  $F_2$  measurement at medium  $Q^2$ .  $x$

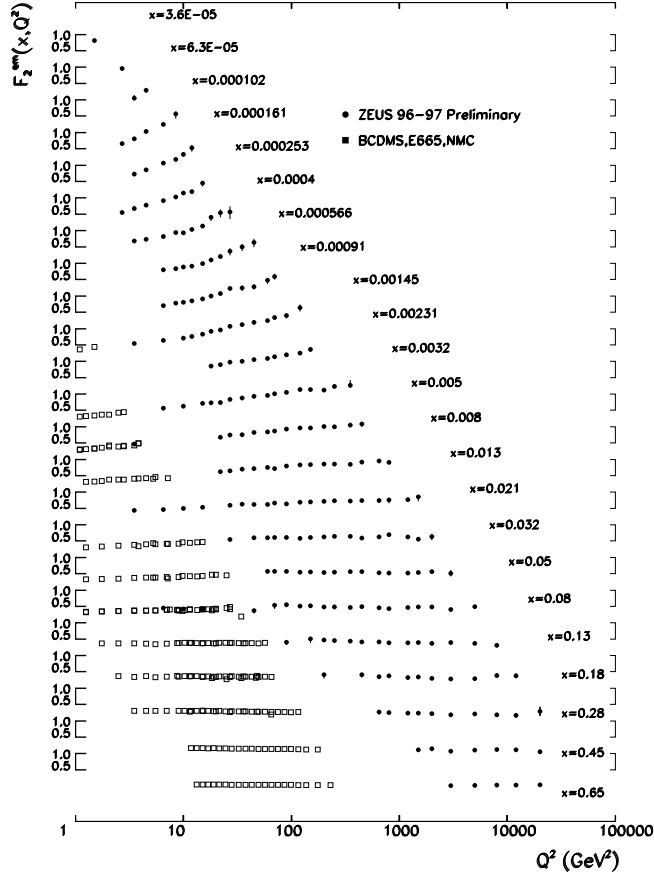


FIG. 8. ZEUS 1996 1997  $F_2$  measurement for all  $x$  and  $Q^2$ . This plot highlights the rise in  $F_2$  as  $x$  decreases.

- 
- [1] ZEUS Collaboration, J. Breitweg et al., Phys.Lett. B407 (1997) 432..
  - [2] B. Badelek, J. Kwiecinski and A. Stasto, Z. Phys. C74 (1997) 297.
  - [3] ZEUS Collaboration, The ZEUS Detector Status Report, DESY 1993.
  - [4] A. Donnachie and P. Landshoff, Z. Phys. C61 (1994) 139.
  - [5] G. Gurci, W. Furmanski and R. Petronzio, Nucl. Phys. B175 (1980) 27;  
W. Furmanski and R. Petronzio, Phys. Lett. 97B (1980) 437 and Z. Phys. C11 (1982) 293.
  - [6] ZEUS Collaboration, M. Derrick et al., Z.Phys. C72 (1996) 399.
  - [7] M. Glück, E. Reya and A. Vogt, Z.Phys. C67 (1995) 433.
  - [8] G. Parisi, Proc 11th Rencontre de Morionde (1976);  
G. Altarelli and G. Parisi, Nucl. Phys. B126 (1977) 298;  
V. Gribov and L. Lipatov, Sov. Jour. Nucl. Phys. 15 (1972) 438;  
L. Lipatov, Sov. Jour. Nucl. Phys. 20 (1975) 94;  
Y. Dokshitzer, Sov. Phys. JETP 46 (1977) 641;
  - [9] A.D. Martin, R.G. Roberts and W.J. Stirling, Phys. Lett. B387 (1996) 419.